J Neurophysiol 126: 1536–1546, 2021.
First published September 22, 2021; doi:10.1152/jn.00203.2021

american physiological society

JNP JOURNAL OF NEUROPHYSIOLOGY

RESEARCH ARTICLE

Sensory Processing

The specificity of orientation-tuned normalization within human early visual cortex

Michaela Klímová,[1,2] Ilona M. Bloem,[1,2,3] and Sam Ling[1,2]

[1]*Department of Psychological and Brain Sciences, Boston University, Boston, Massachusetts;* [2]*Center for Systems Neuroscience, Boston University, Boston, Massachusetts; and* [3]*Department of Psychology, New York University, New York City, New York*

Abstract

Normalization within visual cortex is modulated by contextual influences; stimuli sharing similar features suppress each other more than dissimilar stimuli. This feature-tuned component of suppression depends on multiple factors, including the orientation content of stimuli. Indeed, pairs of stimuli arranged in a center-surround configuration attenuate each other's response to a greater degree when oriented collinearly than when oriented orthogonally. Although numerous studies have examined the nature of surround suppression at these two extremes, far less is known about how the strength of tuned normalization varies as a function of continuous changes in orientation similarity, particularly in humans. In this study, we used functional magnetic resonance imaging (fMRI) to examine the bandwidth of orientation-tuned suppression within human visual cortex. Blood-oxygen-level-dependent (BOLD) responses were acquired as participants viewed a full-field circular stimulus composed of wedges of orientation-bandpass filtered noise. This stimulus configuration allowed us to parametrically vary orientation differences between neighboring wedges in gradual steps between collinear and orthogonal. We found the greatest suppression for collinearly arranged stimuli with a gradual increase in BOLD response as the orientation content became more dissimilar. We quantified the tuning width of orientation-tuned suppression, finding that the voxel-wise bandwidth of orientation tuned normalization was between 20° and 30°, and did not differ substantially between early visual areas. Voxel-wise analyses revealed that suppression width covaried with retinotopic preference, with the tightest bandwidths at outer eccentricities. Having an estimate of orientation-tuned suppression bandwidth can serve to constrain models of tuned normalization, establishing the precise degree to which suppression strength depends on similarity between visual stimulus components.

NEW & NOTEWORTHY Neurons in the early visual cortex are subject to divisive normalization, but the feature-tuning aspect of this computation remains understudied, particularly in humans. We investigated orientation tuning of normalization in human early visual cortex using fMRI and estimated the bandwidth of the tuned normalization function across observers. Our findings provide a characterization of tuned normalization in early visual cortex that could help constrain models of divisive normalization in vision.

divisive normalization; fMRI; vision; visual cortex

INTRODUCTION

Our visual system is tasked with representing our environment as completely as possible while incurring the lowest possible metabolic cost. To accomplish this, the brain relies on gain control mechanisms, which are believed to play an essential role in reducing redundancy in neural coding (1–4). One of the signature examples of gain control in action is surround suppression, wherein the response of a visual neuron to a stimulus is divisively normalized by the sum of activity generated by the stimulus and that generated by a pool of neighboring neurons (5). Divisive normalization not only demonstrably shapes visual responses (5–13), but also plays a role in other sensory systems (14) and higher-level cognitive processes (15), and has become regarded as a canonical neural computation (1).

Correspondence: M. Klímová (mklimova@bu.edu).
Submitted 3 May 2021 / Revised 20 September 2021 / Accepted 20 September 2021

Within visual cortex, the strength of normalization is modulated by stimulus features, and depends on the degree of feature similarity (12). Indeed, normalization-driven suppression has been shown to be strongest when stimuli in the inhibitory surround share similar orientation content to that of stimuli in the excitatory center (12, 13, 16–20). This unique orientation-tuned property of normalization has been proposed to contribute to the efficient neural coding of figure-ground segmentation in visual scenes. In natural scenes, feature discontinuities tend to indicate borders between objects, whereas regions with high feature similarity are often close to each other and belong to the same object (3, 21). Orientation-tuned normalization is believed to play a key supporting role in the efficient coding of neural representations, compressing the amount of neural resources coding redundant collinearities and instead dedicating more vigorous neural responses to discontinuities in orientation, which typically signify areas of visual salience, such as the border between figure and ground (22, 23).

Despite evidence supporting orientation-tuned normalization in the visual cortex of animals (10, 18, 24), investigations in humans mostly focus on contrasting responses to just two cases at the extremes of orientation similarity: collinear and orthogonal stimuli (7, 16, 25–31). In fMRI, stronger suppression for collinearly configured stimuli, compared with orthogonal configurations, has been demonstrated using center-surround grating displays (27, 29, 31), flanker displays (7, 26, 28, 30), and overlapping gratings (16, 25), establishing that BOLD signal suppression from surrounding stimuli is context dependent. However, such comparisons do not allow for closer characterization of this feature-tuned aspect of normalization, for which one would need to parametrically manipulate stimulus orientation differences in finer steps. Capturing the bandwidth, or specificity, of tuned normalization could improve existing models of divisive normalization by estimating the degree of feature similarity required to engage suppression beyond a simple collinear-orthogonal distinction. To our knowledge, no human neuroimaging studies have characterized the specificity of orientation feature tuning. A narrow bandwidth, or high specificity, would suggest that only a small deviation in orientation similarity is sufficient to decrease suppression strength to produce a noticeable change in the BOLD response. On the other hand, a broad bandwidth would suggest that a large change in orientation similarity is needed to modulate suppression strength and BOLD responses. The goal of our experiment was to provide a thorough investigation of the specificity of these feature-selective properties in humans.

In this study, we used functional magnetic resonance imaging (fMRI) to characterize the orientation bandwidth of tuned normalization. To measure orientation-tuned normalization on a large population scale, rather than use a typical center-surround configuration, we designed full-field circular stimuli consisting of wedge-shaped components containing orientation information, and manipulated the orientation differences between the neighboring stimulus components. The extent to which the differently oriented components suppress each other depended on the bandwidth of orientation-tuned suppression. Our results revealed a gradual decrease in BOLD response as orientation similarity increases. We characterized the bandwidth within and across early visual areas V1–V3 by fitting Gaussian functions to the data at the visual area level as well as at the level of individual voxels. Interestingly, the estimate of cortical bandwidths for tuned suppression dovetails nicely with known natural scene statistics (32), supporting efficient coding approaches according to which the visual system is adapted to natural scene statistics (4, 33).

MATERIALS AND METHODS

Observers

The study was approved by the Boston University Institutional Review Board. Ten observers (6 female) participated in the experiment, each completing two scan sessions. An additional observer took part but was excluded from the study after the first session due to poor behavioral performance (fixation task accuracy $< 75\%$; see behavioral performance in *Procedure*). All observers reported normal or corrected-to-normal vision. All were between the ages of 18 and 40, provided written informed consent, and received monetary compensation for their participation, with the exception of two observers who were the authors of the study.

Apparatus and Stimuli

Stimuli were generated using the Psychophysics toolbox in MATLAB (R2015b) on a MacBook Pro (OS X v. 10.10.5), and displayed on a rear-projection screen with a gamma-corrected projector (ProPixx DLP LED, VPixx Technologies). The circular stimulus had an outer diameter subtending 17 degrees visual angle (dva) and inner diameter 3 dva. At the innermost display eccentricity (1.5 dva from central fixation), each wedge subtended roughly 0.47 dva, and at the outermost eccentricity, each wedge subtended 2.66 dva. Stimuli were generated by orientation and spatial frequency bandpass filtering white noise, keeping only spatial frequencies between 2 and 3 cycles/° and the specified orientations, with an orientation filter bandwidth of 10°. Stimuli were presented at 50% Michelson contrast, on a mean luminance background.

We generated stimuli containing 20 wedges in two interleaved sets of 10, with seven possible equally spaced orientation differences between the two sets (0°, 15°, 30°, 45°, 60°, 75°, and 90°; Fig. 1). To avoid strictly orientation-specific effects in our data, we used six different "base" orientations (0°, 18°, 36°, 54°, 72°, and 90°); these orientations also track the angular values of the individual wedges. All stimuli were generated starting from 0° orientation, which we designated as vertical; a "change in base orientation" means that the entire stimulus was rotated by the new base orientation value. For instance, if the orientation difference was 30° and the base orientation was 18° in a given condition, the actual orientation content of the two sets of wedges would be 18° and 48°, maintaining the 30° orientation difference but varying the starting orientation. The orientation content of the wedges (which orientation is displayed within which set of 10) was also counterbalanced; for example, if the orientation difference was 15° and the base orientation was 0°, this condition would be presented four times during each session such that the sets of 10 wedges containing each orientation were switched twice between the four blocks of that specific

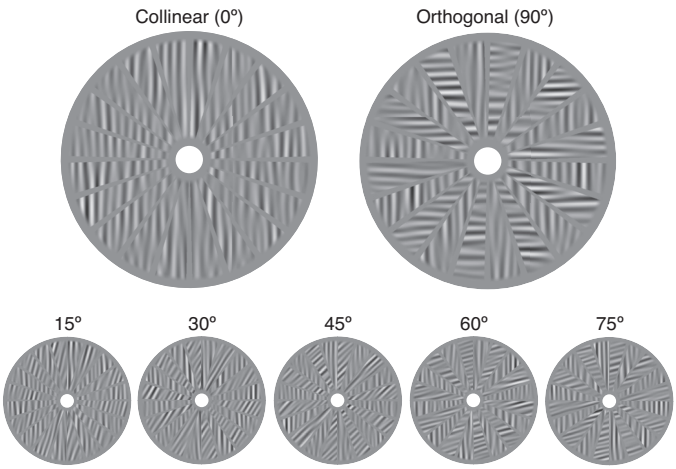

Figure 1. Examples of bandpass filtered stimuli used in the study. The full-field stimuli were composed of two interleaved sets of 10 wedges, filled with two independent noise patches. Stimuli are modified (increased contrast and decreased spatial frequency) for illustration purposes.

condition (combination of orientation difference and base orientation). The white noise patches within each half of the stimulus were independent of each other.

Procedure

Data were acquired at the Cognitive Neuroimaging Center at Boston University using a 3.0 Tesla Prisma scanner (Siemens, Erlagen, Germany) with a 64-channel head coil. All participants underwent two scanning sessions, each lasting between 2 and 2.5 h. In each session, observers completed 14 functional scan runs (with the exception of one who only completed 11 runs in one of their sessions) with the acquisition field of view oriented perpendicular to the calcarine sulcus [T2*-weighted in-plane multislice imaging sequence with multiband factor 3 (34, 35), 36 slices, TR = 1 s, TE = 35.4 ms, flip angle = 64°, FoV = 136 mm, voxel size = 2 mm isotropic]. An anatomical scan used to register the functional data was acquired during a separate session (T1-weighted multi-echo MPRAGE 3-D sequence, voxel size = 1 mm isotropic, FoV = 256 × 256 × 176 mm, TR = 2,530 ms, TE = 1.69 ms, flip angle = 7°).

Stimuli were presented in a block design (14 s on, 14 s off). Each functional run lasted 350 s (1 s TR) and contained 12 stimulus blocks. Each set of 14 runs contained 24 repetitions of each orientation difference condition, fully counterbalanced to reach equal numbers of base orientation presentations. The noise patch underlying the orientation stimulus was refreshed at 2 Hz, whereas within each stimulus block of the run, the orientation condition remained unchanged. Throughout the run, participants were required to maintain central fixation and perform a letter discrimination task within the fixation circle. The fixation circle subtended 0.8 dva and contained a stream of letters, refreshing every 250 ms. Participants' task was to detect letters "J" and "K" within this distractor letter stream and press a corresponding key on a two-button response box for each target letter as soon as it was detected. The letter detection/discrimination task was employed throughout the run in both baseline and stimulus blocks, and targets could appear at any point during the run (regardless of baseline or stimulus block). Behavioral performance in the fixation letter detection task averaged 93.2% accuracy (±1.86% SE), confirming that our observers were well able to maintain alert fixation throughout the scan session. Before acquiring the task scans, participants underwent two runs of a functional localizer (14 s on, 14 s off, 182 TRs total), later used for voxel selection. The localizer stimulus was composed of a 100% Michelson contrast spatial pattern flickering at a rate of 10 Hz. The localizer stimulus had identical inner and outer eccentricity bounds to the experimental stimulus and encompassed the entire stimulus display (rather than split into individual wedges). The spatial pattern of the localizer was created by summing and rectifying pairs of spiral and radial gratings. Throughout localizer presentation, participants were engaged in a fixation task identical to the main experiment. In both the main task and localizer, each scan always began and ended with an off-block.

fMRI Data Analysis

Population receptive field mapping and voxel selection.
Population receptive field (pRF) mapping was conducted for each participant in a separate session, using the analyzePRF toolbox for MATLAB (36, 37). In the pRF session, observers were presented with two to three scans of each of two types of mapping run: expanding/contracting ring and bar sweep stimuli, and rotating wedge stimuli. The stimuli were composed of a pink noise background with color objects and faces of varying spatial scale, on a display with mean luminance background (36, 38). These are the same stimuli as the ones used in the Human Connectome Project 7 T Retinotopy dataset (38). The pink noise and images were refreshed at a rate of 15 Hz. The results were analyzed with analyzePRF, implementing the compressive spatial summation pRF model (37). The results of the pRF analysis were used to manually draw region-of-interest (ROI) labels, defining early visual areas V1, V2, and V3. pRF modeling results were then used in conjunction with the localizer data to select voxels for further analysis. Within each label, we first identified the top 40% most visually responsive voxels across both sessions, based on the localizer data. From this subset, we further excluded voxels whose population receptive fields were located outside the eccentricity bounds of the stimulus, or those whose pRF model fit was poor ($R^2 < 10\%$). On average, this procedure left 446 ± 96 (SD) voxels in V1, 394 ± 62 voxels in V2, and 281 ± 45 voxels in V3 for analysis.

fMRI data preprocessing.
We applied EPI distortion correction to all fMRI BOLD time series data using a reverse-phase encoding method (39) implemented in FSL (40). The field map corrected data from each session were then preprocessed with standard motion correction procedures, Siemens slice timing correction, and boundary-based registration between functional and anatomical spaces (41) implemented in FreeSurfer (42), v. 5.3. No spatial smoothing was applied. To achieve voxel-by-voxel alignment within and between the two experimental sessions, we applied robust rigid registration (43), using the middle time point of each run, and aligned each functional run from both sessions to the first localizer scan in the first session, which had been aligned to the anatomical data in

the boundary-based registration step. Data for each voxel were subsequently detrended, high-pass filtered, and converted to percent signal change using custom MATLAB scripts. The functional localizer data were analyzed separately for each session using a standard GLM analysis in FreeSurfer. The main task data for the two sessions were concatenated and further analyses were performed in MATLAB using custom code.

fMRI data analysis.

For each observer, data were summarized in every voxel by computing an event-triggered average for each orientation difference condition, collapsing across the six base orientations and across repetitions of each condition. To account for hemodynamic delay, a temporal shift of six TRs (6 s) was implemented before averaging, resulting in an averaging window starting at 6 TRs following stimulus onset and ending at 14 TRs (stimulus offset), which captured the peak of the BOLD activity.

Model fitting. We quantified the tuned normalization parameters in two ways: on the ROI-averaged data, and in individual voxels. To obtain the ROI mean, we averaged across all voxels within each ROI for each observer, and performed the fitting procedure described in this section for each ROI and observer. In individual voxels, model fitting was done on each voxel's averaged response. To quantify the tuned normalization parameters, the data were fit with a half Gaussian function centered on an orientation difference of 0°:

$$Response = b + Ae^{\frac{-(X-\mu)}{2\sigma^2}},$$

where b refers to the baseline BOLD activation, A is the amplitude or the peak of the function, μ is the mean of the function (set to 0° in order to constrain the fit), and σ is the standard deviation, which we will use as an estimate of bandwidth. For each voxel or ROI, the Gaussian was fit to the 7 BOLD response values for each orientation difference by minimizing least-squared error using the MATLAB *fmincon* function. The bandwidth parameter was constrained between 5° and 90°; this was done to avoid distortions caused by voxels that either showed no tuning to orientation difference (resulting in a flat response function) or unreasonably narrow tuning. Furthermore, due to the orientation filter bandwidth of 10° (5° on either side of the target orientation), the actual minimum possible angular difference between individual orientation segments in two components was 5° (in the 15° orientation difference condition). The overall response amplitude was constrained by an upper bound of 10% signal change; no constraints were applied to the baseline parameter. We subsequently calculated the R^2 values of the predicted Gaussian fit for each voxel. The minimization procedure converged on a solution for all fits and initially no data were excluded following fitting (but see RESULTS).

We additionally computed a suppression strength metric from the raw data, expressed in units of % signal change. In the whole-ROI analyses, we defined suppression strength in each ROI as the difference between the averaged BOLD response in the orthogonal condition and the collinear condition. In the individual voxel analyses, suppression strength was defined as the difference between each voxel's average BOLD response in the orthogonal configuration and that in the collinear configuration.

Statistical tests were implemented in MATLAB and R using custom scripts. For statistical comparisons across observers, unless stated otherwise, we ran a repeated-measures ANOVA with visual area as grouping factor (observers were treated as random variables), and applied Bonferroni correction for the number of visual areas to all post hoc t tests. When conducting one-sample t tests separately within individual ROIs, no corrections were applied. Unless stated otherwise, we report measures of dispersion as means ± standard error (SE).

Data and code availability.

Preprocessed fMRI data, behavioral data, and stimulus and data analysis scripts used to generate the results and figures in this manuscript can be found on the Open Science Framework website (https://osf.io/bcyp5/).

RESULTS

Tuned Normalization Bandwidth: Whole ROI Analyses

Consistent with existing literature (7, 16, 25–31), collinear stimuli evoked lower amplitude BOLD responses compared with orthogonal stimuli. Suppression strength (the difference between averaged BOLD responses in the orthogonal condition and that in the collinear condition) was largely positive, except in a single ROI for one of the 10 observers. The average suppression strength was 0.23 ± 0.05 in V1, 0.28 ± 0.05 in V2, and 0.2 ± 0.05 in V3. There was a significant main effect of visual area [$F_{(2,18)}$ = 6.559, P = 0.007]; post hoc t tests revealed this reflected a significant difference between suppression strength in V2 and V3 [$t_{(9)}$ = 4.58, P = 0.004]. Suppression strength in each ROI differed significantly from 0 [one-sample t tests, V1: $t_{(9)}$ = 4.6, P = 0.001, V2: $t_{(9)}$ = 5.16, $P < 0.001$, V3: $t_{(9)}$ = 3.96, P = 0.003]. Importantly, for the majority of observers, and for all three visual areas V1/V2/V3, BOLD response magnitude showed a clear gradual increase as a function of orientation difference (Fig. 2), indicating that suppression strength changes progressively as a function of the degree of orientation similarity. Note that as the data plotted in Fig. 2 are normalized with respect to the response in the orthogonal condition, the values listed above do not directly correspond to the differences observed in Fig. 2. To characterize the overall orientation-tuned normalization response, we averaged across all voxels in each ROI and observer, and fit the data individually (per observer and ROI) with a half-Gaussian function. An example of fits for a representative observer are shown in Fig. 3. With these fits, we obtained an estimate of the standard deviation (bandwidth), amplitude, and baseline for each observer and ROI. Note that due to the shape of the tuned normalization function, the fit is an inverted Gaussian, therefore decreasing in amplitude toward the mean. As a result, the baseline parameter represents the upper bound of the Gaussian fit, and the amplitude represents the difference between the baseline and the y-intercept of the curve (which corresponds to BOLD response magnitude of the collinear condition), and has a negative value for all observers. The amplitude parameter is closely related to suppression strength, as it is the difference between the fitted responses to collinear and orthogonal

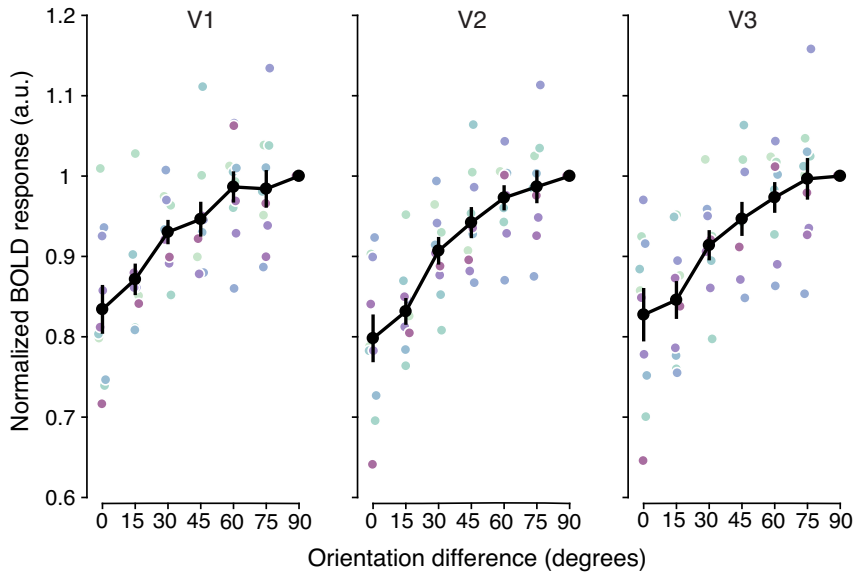

Figure 2. BOLD responses as a function of orientation difference, across observers (n = 10), from V1–V3. Responses for each observer were normalized with respect to the response to the 90° orientation difference condition. Thick black line represents the observer average of these normalized responses. Colored points depict responses for individual observers. Error bars represent means ± 1 SE.

conditions, while suppression strength is the difference between the actual BOLD responses in those two conditions. Therefore, more negative amplitude estimates and larger suppression strength point to greater suppression (larger difference between the collinear and orthogonal ends of the fitted Gaussian curves). The baseline is an additive parameter included to account for different absolute BOLD signal change magnitudes across observers and ROIs. We largely focus on our measures of suppression strength, and the Gaussian parameter estimates of bandwidth and amplitude for the remainder of the analyses.

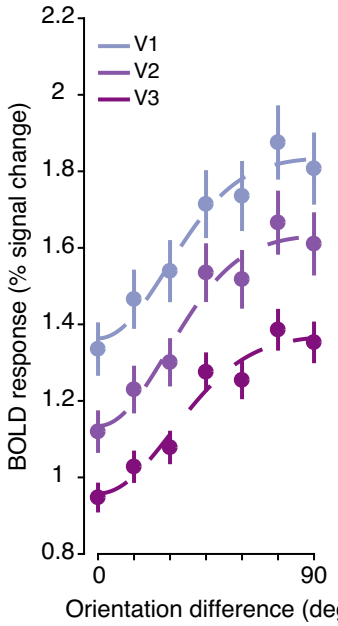

Figure 3. Gaussian function fit to the tuned normalization data for a single example observer. Points indicate the average BOLD signal for each region-of-interest (ROI) means ± 1 SE. Dashed lines represent the Gaussian fits for each ROI for this representative participant.

The Gaussian fit the data well (average R^2 0.66 ± 0.11 in V1, 0.8 ± 0.08 in V2, and 0.73 ± 0.08 in V3), enabling us to rely on the standard deviation parameter as a proxy for tuned normalization tuning width estimates. Using this approach, we found that the average bandwidth was 42.3° ± 10.5° in V1, 32.7° ± 6.7° in V2, and 34.7° ± 7.6° in V3. Observer-averaged estimates of the parameters are displayed in Fig. 4*A*. R^2 values are included in Supplemental Fig. S1 (https://doi.org/10.6084/m9.figshare.15826077). There were no between ROI statistical differences in the bandwidth parameter [$F_{(2,18)}$ = 1.422, P = 0.27], or the amplitude parameter [$F_{(2,18)}$ = 1.56, P = 0.24]. The baseline parameter was significantly different between visual areas [$F_{(2,18)}$ = 13.18, $P < 0.001$], reflecting lower BOLD responses in area V3 (1.07 ± 0.08% signal change) compared to V1 and V2 [1.36 ± 0.1%; $t_{(9)}$ = 5.18, P = 0.002 and 1.32 ± 0.1%; $t_{(9)}$ = 3.82, P = 0.012, respectively; see Fig. 3]. There was also considerable interobserver variability in the bandwidth parameter. As can be seen in Fig. 4*A*, the average is slightly inflated due to a few observers whose BOLD response did not show strong orientation-tuned suppression, resulting in a flat function.

Tuned Normalization Bandwidth: Voxel-Level Analyses

Model fitting and voxel exclusion.

We then carried out the fitting procedure at the individual voxel level for each observer and ROI. The median for each parameter estimate was computed and averaged across observers. Averaged median R^2 was 0.52 ± 0.07 in V1, 0.59 ± 0.07 in V2, and 0.52 ± 0.06 in V3, reflecting the increased noisiness in the single-voxel data, as compared with ROI averages. As with the ROI-averaged data, there were no significant differences between ROIs in the bandwidth parameter [$F_{(2,18)}$ = 0.7, P = 0.51]. There was a main effect of ROI in the baseline parameter [$F_{(2,18)}$ = 13.65, $P < 0.001$], again reflecting differences between V1 (1.05 ± 0.07% signal change) and V3 (0.87 ± 0.07% signal change; $t_{(9)}$ = 4.74, p = 0.003] and V2 (1.07 ± 0.08% signal change) and V3 [$t_{(9)}$ = 5.53, P = 0.001]. We also observed a main effect of ROI in the amplitude parameter [$F_{(2,18)}$ = 5.57, P = 0.013], which reflected

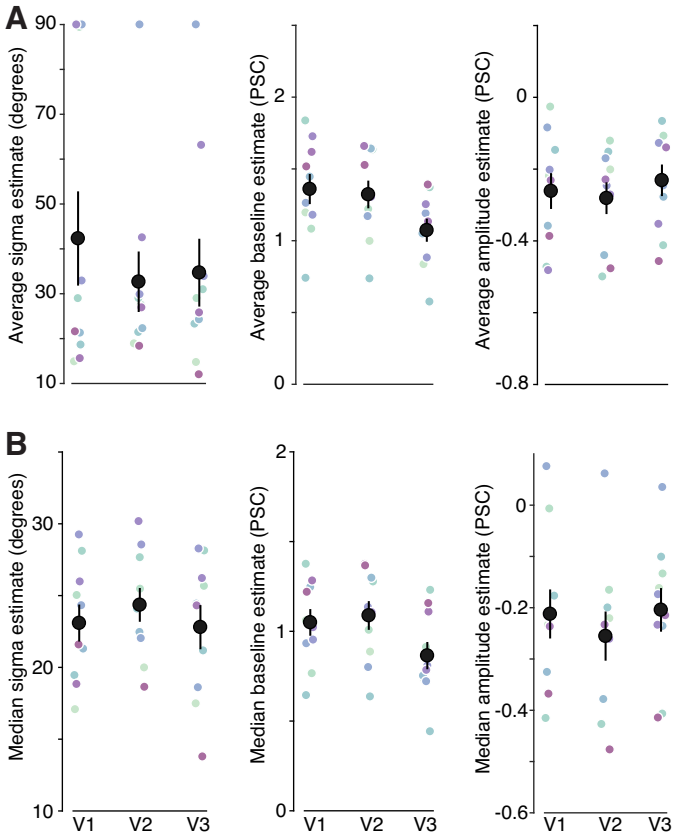

Figure 4. *A*: parameter estimates (n = 10) for all visual areas, obtained by fitting region-of-interest (ROI)-averaged voxel activation values for each observer and ROI (PSC, percent signal change). *B*: median (per observer/ROI) parameter estimates for all visual areas following removal of voxels whose sigma parameter was estimated to be wider than 85° (n = 10). Data are shown as observer averages ± 1 SE. Colored points represent individual observer parameter estimates whereas large black circles represent the observer averages.

marginally significant differences between V1 and V2 [$t_{(9)}$ = 2.95, P = 0.049] and differences between V2 and V3 [$t_{(9)}$ = −3.38, P = 0.025]; amplitude was lower in V2 than in the other visual areas (−0.28 ± 0.04 in V2 vs. −0.23 ± 0.04 in V1 and −0.23 ± 0.04 in V3). There was large variation in the bandwidth estimates between observers, but also between individual voxels. Specifically, a number of voxels showed weak orientation-tuned suppression, meaning that their estimated sigma value fell exactly below the upper boundary of 90° and their BOLD response remained largely flat across orientation differences, compared to the remaining voxels. Upon further inspection, the voxels in question also showed overall lower R^2 values (V1: 0.26 ± 0.04, V2: 0.31 ± 0.06, V3: 0.28 ± 0.04), and weaker overall responses (lower BOLD % signal change; Supplemental Fig. S2; https://doi.org/10.6084/m9.figshare.15830391). To obtain a clearer picture of those voxels which did show tuning, we excluded a subset of voxels whose sigma estimate fell above 85°, capturing those that lacked tuning and had the maximum possible standard deviation (see Supplemental Fig. S3 at https://doi.org/10.6084/m9.figshare.15830526 for the distributions of bandwidths across all voxels and observers). This led to the removal of 26.7% (± 4.5%) of voxels on average in V1, 22.7% (± 4.3%) in V2, and 26% (± 4.2%) in V3. We then computed within-ROI median and observer-average estimates from the remaining voxels, shown in Fig. 4*B*. Voxel exclusion resulted in an overall increase in R^2 compared with a voxel-wise analysis with all voxels included (V1 average: 0.58 ± 0.06, V2: 0.64 ± 0.06, V3: 0.58 ± 0.06) and a decrease in the sigma parameter average, but did not qualitatively change the overall results, which found no differences between visual areas in bandwidth [$F_{(2,18)}$ = 1.4, P = 0.27]. There was again a main effect of ROI in the baseline parameter [$F_{(2,18)}$ = 12.4, P < 0.001], with significant post hoc t tests in comparisons between V1 and V3 [V1: 1.05 ± 0.07, V3: 0.86 ± 0.08; $t_{(9)}$ = 3.53, P = 0.019], and V2 and V3 [V2: 1.09 ± 0.08; $t_{(9)}$ = 4.74, P = 0.003]. The amplitude parameter also differed between areas [$F_{(2,18)}$ = 4.7, P = 0.023], this time with a significant post hoc test only in V2 versus V3 [V2: −0.26 ± 0.05, V3: −0.2 ± 0.04; $t_{(9)}$ = −3.39, P = 0.024]. As there was high similarity between the statistical comparisons in these two samples, subsequent analyses were carried out using the voxel subset with stricter selection criteria of SD < 85°. The tuning width (standard deviation) estimates obtained with this voxel subset were 23.1° ± 1.3° in V1, 24.4° ± 1.2° in V2, and 22.8° ± 1.5° in V3, calculated by averaging ROI-median estimates within ROI across observers.

Voxel-wise suppression strength was positive for the majority of voxels. The observer-averaged suppression strength (calculated as average of each observer's ROI medians) was somewhat lower compared to the whole-ROI averages; 0.2 ± 0.04 in V1, 0.23 ± 0.05 in V2, and 0.16 ± 0.04 in V3. There was again a significant main effect of visual area on suppression strength [F(2,18) = 6.53, P = 0.007], reflecting lower suppression strength in V3 compared with V2 [$t_{(9)}$ = 4.27, P = 0.006], results consistent with the ROI average. One-sample t tests again showed that suppression strength in each ROI was significantly different from 0 [V1: $t_{(9)}$ = 4.62, P = 0.001, V2: $t_{(9)}$ = 4.99, P < 0.001, V3: $t_{(9)}$ = 3.6, P = 0.006].

As an additional analysis to validate the correspondence between amplitude and suppression strength, we conducted a Spearman correlation between voxel-wise amplitude estimates and suppression strength in each observer and ROI. The observer-averaged correlation coefficients were −0.85 (± 0.03) in V1, −0.87 (± 0.02) in V2, and −0.87 (± 0.02) in V3, indicating strong correspondence, where more negative amplitudes (representing larger differences between the fitted 90° response and the fitted 0° response) track larger suppression strengths.

Tuned suppression and voxel spatial preference.

To further investigate properties of tuning width and suppression strength, we carried out additional exploratory analyses to characterize any dependence of suppression strength or the fitted parameters on voxels' retinotopic preference. To examine retinotopic preference dependencies, we binned the voxels into 8 eccentricity bins, logarithmically spaced between 1.5° and 8.5° (the inner and outer limits of the stimulus, respectively), collapsed across polar angle preference (Fig. 5). Following this, we computed the median estimate for each parameter per bin, observer and ROI. For each ROI and observer, we then fit a linear function through the data. Averages of the slope estimates were subsequently

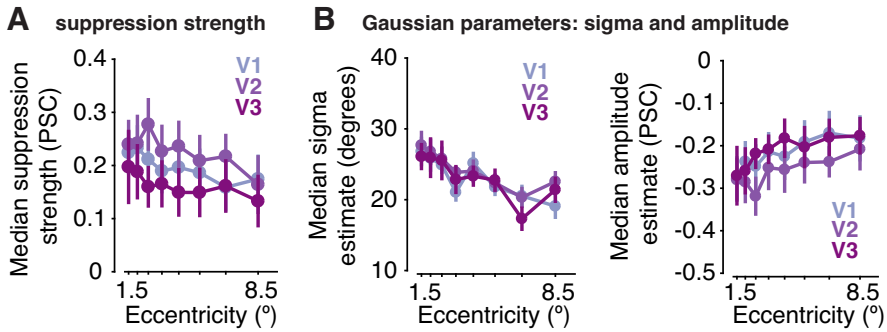

Figure 5. Relationship between data-derived suppression strength and eccentricity ($n = 10$; PSC, percent signal change; *A*) the Gaussian parameter estimates sigma (*middle*) and amplitude (*right*) vs. eccentricity ($n = 10$; *B*). The data points represent observer means of the parameters ± 1 SE, per region-of-interest (ROI) and eccentricity bin.

computed across observers. We assessed the relationship between the parameters and eccentricity by submitting the slopes for each ROI to a one-sample *t* test. The slope for the σ parameter was found to be significantly different from zero in all 3 ROIs [slopes: −1.2 ± 0.29 in V1, $t_{(9)} = -4$, $P = 0.003$; −1.02 ± 0.31 in V2, $t_{(9)} = -3.3$, $P = 0.009$; −1.14 ± 0.39 in V3, $t_{(9)} = -2.9$, $P = 0.018$], indicating that the tuning width of tuned normalization decreases with increasing eccentricity. The averaged slopes for amplitude and suppression strength were not significantly different from zero in any of the ROIs.

We further explored whether these relationships also depend on polar angle, as previous work has shown that perceptual processing can differ between visual field segments, for example between upper and lower visual fields (44–46). We separated the visual field into quadrants, each comprising 90° above, below, left, and right of fixation. Within each visual field segment, we averaged the median estimates across eccentricity bins for each observer and ROI to look for differences between visual field segments. As can be seen in Fig. 6, there appeared to be significant differences in suppression strength between the upper and lower visual fields [paired *t* tests; V1 $t_{(9)} = 4.17$, $P = 0.002$; V2 $t_{(9)} = 7.83$, $P < 0.001$; V3 $t_{(9)} = 2.65$, $P = 0.026$), where suppression strength is generally stronger in the upper visual field (0.31 ± 0.06 in upper visual field vs. 0.19 ± 0.04 in lower visual field); this relationship holds in all three ROIs. We also found amplitude differences across the three ROIs between upper and lower quadrants: higher amplitude estimates were observed in the lower visual field across ROIs [paired *t* tests; V1 $t_{(9)} = -3.58$, $P = 0.006$; V2 $t_{(9)} = -8.3$, $P < 0.001$; V3 $t_{(9)} = -3.27$, $P = 0.01$]. The average amplitude in the upper visual field was −0.35 ± 0.05 and −0.22 ± 0.05 in the lower visual field. As mentioned earlier, more negative amplitude estimates, together with larger suppression strength, indicate a stronger suppression effect in this area of the visual field. Generally, we did not observe reliable differences in bandwidths between visual field segments; only in V2, in the comparison between left and right visual field, was there a statistically significant difference [$t_{(9)} = -3$, $P = 0.015$], with wider sigma in the right visual field. Plots depicting slopes between the left and right quadrants of the visual field are shown in Supplemental Fig. S4 (https://doi.org/10.6084/m9.figshare.15830532). In addition, we have included surface maps for polar angle, eccentricity and bandwidth for our representative observer in Supplemental Fig. S5 (https://doi.org/10.6084/m9.figshare.15830538).

In an additional exploratory analysis, we asked whether the position of a voxel on the wedge had an influence on suppression strength. Most differential suppression in our stimulus was thought to occur at the boundary regions between adjacent wedge components; each wedge serves as a "center" as well as a "surround" in this circular full-field arrangement. One could therefore assume that suppression strength might differ between portions of our participants' visual fields corresponding to the boundaries between wedges and the inner surfaces of the wedge components—specifically, that we would find tuning by orientation difference at the boundaries of the wedges but not on the surfaces of the components where the orientation content is always collinear. To explore this possibility, we binned voxel polar angle estimates from the pRF analysis according to their position on the wedge, into 1° bins, as follows: first, we split each wedge into 18 bins (as each wedge spanned 18°) and grouped voxels from corresponding bins in each of the 20 wedges together. We then grouped them based on the distance from the

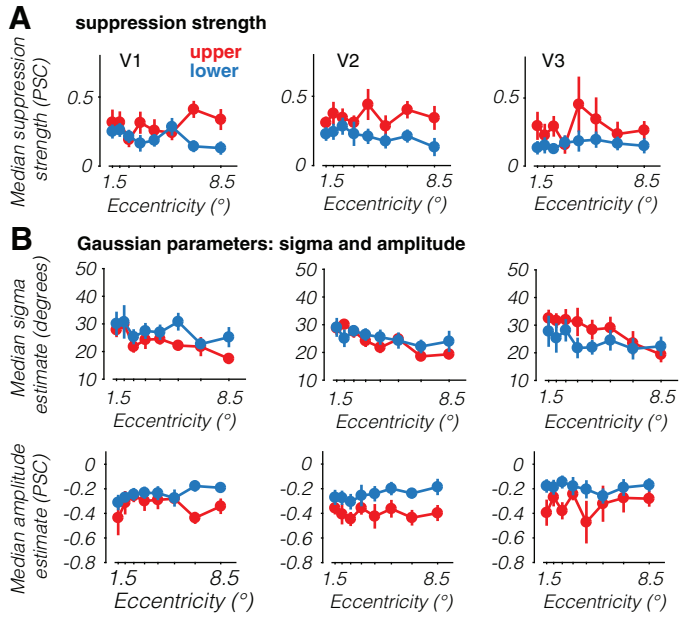

Figure 6. Visual field differences in tuned normalization. *A*: median suppression strength ($n = 10$; PSC, percent signal change). *B*: standard deviation (*top*) and amplitude (*bottom*), $n = 10$. Points represent means across observers ± 1 SE plotted as a function of eccentricity, separated by visual field segment. Each panel shows the comparison between upper visual field (*top*; red) and lower visual field (*bottom*; blue).

boundary, as opposed to just position on the wedge; for example, voxels from the 0°–1° bin and 17°–18° bin were now in the same group, as both are equally distant from the boundary of the wedge. This step produced 9 bins (0°–1° from boundary, up until 8–9-degree from boundary, which was the center of the wedge). For each ROI and observer, we then took the median of estimates for all voxels in each bin, and averaged over observers for each ROI. We then fit a simple linear model to the observer-averaged data in each ROI. Distance from boundary did not act as a significant predictor for suppression strength or any of the Gaussian parameters (See Supplemental Fig. S6, https://doi.org/10.6084/m9.figshare.16617658). That is not to say there is no potential spatial gradient, but our particular wedge and border sizes were likely too small given the estimated pRF sizes of our voxels, to pick up on these presumably finer scale gradients in suppression strength. We designed our stimulus to elicit the most suppression on a large population scale, and to maximize the number of voxels differentially modulated by suppression throughout the display. Thus, the wedges took up 0.47 dva at the innermost stimulus eccentricity and 2.66 dva at the outermost eccentricity (see MATERIALS AND METHODS), while the "gaps" between the components took up less than 0.1 dva at all eccentricities. On the other hand, the observer-averaged median estimates of voxel receptive field sizes were much larger than the gap sizes (in the closest eccentricity bin—V1: 0.43 ± 0.01 dva, V2: 0.53 ± 0.05 dva, V3: 0.61 ± 0.03 dva; in the highest eccentricity bin—V1: 0.75 ± 0.1 dva, V2: 1.6 ± 0.06 dva, V3: 2.1 ± 0.13 dva).

A final exploratory analysis examined potential causes of broad bandwidth estimates in the excluded voxels, namely that they may be caused by noisy voxels, as indicated by the Gaussian R^2. As expected, there were significant negative correlations between bandwidth and R^2 (Spearman correlation, observer-averaged correlation coefficients −0.25 ± 0.03 in V1, −0.23 ± 0.04 in V2, and −0.24 ± 0.03 in V3); this agrees with our above observation of overall lower average R^2 values in broad-bandwidth voxels. We first looked at the spatial distribution of these voxels across the stimulus display. Broad bandwidth voxels were found across the entire visual field, as opposed to being bound to e.g., only high eccentricities, suggesting that broad bandwidth fitting in these voxels was not an artifact of their visual field position. We subsequently examined the behavior of bandwidth and R^2, in all the voxels that underwent the Gaussian fitting, across the visual field; if broad bandwidths were simply a product of lower R^2, we would expect corresponding behavior of the two parameters, i.e., as bandwidth becomes sharper towards the periphery, we would expect higher R^2 values there. However, this was not the case; we binned R^2 and bandwidth for the whole voxel set into eccentricity bins, following the same steps we took in creating Fig. 5. Although R^2 tended to decrease with eccentricity [slope was significantly different from 0 in V3, $t_{(9)} = -2.62$, $P = 0.028$], bandwidth showed a similar pattern as in Fig. 5, with slope significantly different from 0 in V1 [$t_{(9)} = -3.24$, $P = 0.01$], and no increases in slope. This suggests that broad sigma estimates are not entirely a product of low R^2.

DISCUSSION

Our results suggest that the bandwidth of tuned suppression in human early visual cortex is around 23° on average, and between 20° and 30° for most observers. This finding, which to our knowledge is the first fMRI investigation of tuned suppression bandwidth, expands on previous studies showing reliable differences in BOLD signal amplitude between collinear and orthogonal stimulus configurations (7, 16, 25–31).

These findings build on existing animal and psychophysical work, some of which did explore the extent of orientation-dependent tuning of surround suppression. One animal study (18) varied orientation differences in a center-surround stimulus, gradually changing the relative orientations of the two components in 30° increments, and found that response magnitudes decrease incrementally with increasing similarity, although suppression bandwidth was not directly investigated. Shushruth et al. (11) investigated suppression tuning more directly and discovered significant tuning with center-surround stimuli, which they roughly matched between macaque V1 recordings and an accompanying human psychophysical study using contrast matching. Tuning was sharper when the center and surround were in proximity, and weaker when they were far apart. Petrov et al. (17) also used a contrast matching task with center-surround stimuli in humans and reported that surround suppression was quite tightly tuned, with strong suppression at similar orientations and almost no suppression at orientation differences that exceed 45°. Cannon and Fullenkamp (47) concluded there are two tuning mechanisms in their study using a psychophysical contrast matching task with human observers and center-surround stimuli: one suppression mechanism was narrowly tuned, disappearing at an orientation difference of ~15°, whereas the other decreased more gradually and was still present when the center-surround orientation difference reached 90°. Our stimuli are not center-surround, and so we were unable to employ a center-only condition to compare the amount of suppression at 90° with a no-surround configuration. At the same time, our minimum orientation difference was 15° (although see discussion on stimulus limitations below), and so we cannot study the narrower tuning mechanism. However, the BOLD signal strength in our data set continued to change with increasing orientation differences up until a difference of 90°, suggesting some similarity between the mechanism we captured and the broader tuning component reported by Cannon and Fullenkamp (47). More recently a psychophysical study (48) examined the bandwidth of suppression in motion direction tuning by using center and surround grating stimuli which differed in relative orientation as well as motion direction, and found that when motion directions of the center and surround matched, suppression strength was at its maximum, decreasing with increasing angular direction differences. The reported average tuning width for motion direction differences was 28°, which bears close resemblance to our average estimates of tuning for orientation differences.

When comparing our suppression strength results to existing literature, it is important to note that the work presented here measures only the tuned component of suppression, i.e., the difference in BOLD response between collinear and

orthogonal stimulus configurations, whereas most literature examining suppression strength focuses on contrasting BOLD responses to a central stimulus with or without a surround (i.e., untuned suppression). Untuned suppression was generally found to be stronger in extrastriate areas, as compared to V1 (49, 50). Few groups directly examined differences in tuned suppression between visual areas. Bloem and Ling (16) found a decrease in tuned normalization magnitude across early visual areas, while Poltoratski et al. (26), who used flanker displays, reported no statistical differences. Other studies examining tuned normalization did not conduct direct statistical comparisons between areas (27, 30), although one reported that tuned suppression was significantly different from zero in extrastriate cortex but not in V1 (27).

Likewise, in previous psychophysical work, tuned and untuned suppression have shown diverging eccentricity effects. Untuned suppression strength typically increases with eccentricity with a plateau at around 4 dva from fixation (13, 17). However, Xing and Heeger (13) found no eccentricity-based differences in the magnitude of tuned suppression, but noted that suppression was stronger, and less specific, in the visual field periphery. Our neuroimaging results also revealed no eccentricity effects on tuned suppression strength. Unlike previous studies, we did not use a cortical magnification factor to adjust the spatial frequency of our stimuli with eccentricity, which could be a contributing factor for some of the differences bet-ween previous findings and our results. The other obvious difference is the overall stimulus configuration—all previous work described above used center-surround grating stimuli or flanker displays to elicit surround suppression. While our stimulus clearly elicits measurable orientation-tuned responses in the visual cortex, it makes direct comparisons with studies using different stimuli difficult.

A limitation of our stimulus was the orientation filter bandwidth (10°, see MATERIALS AND METHODS). The addition of a filter bandwidth means that the possible orientation differences between individual components could range around the intended value (for instance, in a 15° orientation difference condition where one component is 0° and the other 15°, the filter bandwidth used means that the actual minimum difference between some of the individual components could range between 5° and 25°). While this clearly does not hinder our ability to measure orientation-tuned suppression, it imposes a limit on the precision of bandwidth estimates.

The goal of the present study was to estimate the bandwidth of orientation-tuned suppression, which is distinct from orientation tuning bandwidth. That said, our ability to measure orientation-tuned suppression bandwidth is also limited by the underlying orientation tuning in the visual areas of interest. Orientation tuning bandwidth within human visual cortex has been studied with psychophysics and fMRI. For instance, one study (51) used fMRI adaptation to measure transient BOLD responses to orientation changes in a full-field grating stimulus, and estimated the bandwidth of orientation tuning in human V1 at 45°. In psychophysical work using the orientation noise-masking technique (52), estimated orientation tuning bandwidth ranged between 15 and 30 degrees. Thus, similar to investigations of tuned normalization bandwidth, estimates of orientation tuning bandwidth in human early visual cortex vary quite widely.

Our results could be of use in further constraining current models of divisive normalization so that they take more granular feature similarity into account. The notion that suppression strength varies with feature similarity has been explored in research investigating how the visual cortex appears optimized for natural scene properties. According to theories of efficient coding, the visual system attempts to remove redundancies in incoming visual input to achieve a more efficient representation, and one of the ways this could be accomplished is through divisive normalization (3). Indeed, there is evidence that surround suppression among V1 neurons in the macaque is stronger for homogeneous, as opposed to heterogeneous, images, suggesting that feature tuning supports efficient coding of visual stimuli, discounting less informative homogeneous regions and highlighting contrasts between objects to promote figure-ground segregation (2, 33). Coen-Cagli et al. (2) further demonstrated the significance of feature similarity in divisive normalization by showing that the standard normalization model only accounts for roughly half the variance in macaque V1 neural responses to natural images, but when a gating component based upon the degree of homogeneity in the images was added to the model, the variance explained dramatically improved. In this flexible model variant, when the center and the surrounding portions of an image share their features and are thus considered homogeneous, the surround suppression mechanism is engaged; however, when the two components are judged as heterogeneous, the surround influence is "switched off" and the neural response to the center component of the visual stimulus is not normalized by the response to the surrounding area. While this model improves data fits significantly, incorporation of our more fully characterized surround suppression function could provide an even closer prediction; having knowledge of the bandwidth could allow for a gradual adjustment of suppression strength, and yield an estimate of how much suppression one might expect for a particular orientation difference.

More evidence to support the idea that tuned normalization strength reflects the most common properties of natural scenes comes from natural image statistics analyses. While it was well established that nearby contours are most likely to be collinear (23), Sigman et al. (32) examined the number of occurrences of orientation differences graded in 11.25° steps between image segments, found in a database of 4,000 photographs of natural scenes. Pairs of segments containing orientations collinear to each other occurred most frequently, and there was a gradual drop in frequency with decreasing orientation similarity, with orthogonal orientation segment pairs being least likely to co-occur in a scene, matching our results. This finding squares with our results particularly in light of efficient coding perspectives. The surround region can be thought of as setting the context for the center (3, 30), and when the center matches this expectation (i.e., is collinear), the output of the units responding to the center is suppressed to reduce redundancy in neural coding. Conversely, when the center is orthogonal to the surround, reduced suppression will ensure that this informative signal is processed with increased saliency. This supports

the notion that suppression strength dependence on orientation similarity is well matched to the statistics of natural stimuli; more predictable, redundant components, which are also more likely to co-occur in scenes, are suppressed, while the less frequently occurring stimuli, which often highlight regions of interest such as figure-ground transitions, benefit from increased saliency brought about by reduced suppression.

In summary, our results reveal that suppression strength in human early visual cortex depends on orientation differences between scene elements. Of course, other features play a role in our visual system's ability to parse visual scenes, such as similarities in contrast and spatial frequency, or distance between scene components (2, 47, 53, 54). Here we focused solely on orientation differences, but going forward, incorporating other dimensions, in particular stimulus contrast, would be a crucial next step in fully characterizing the profile of feature-tuned normalization.

SUPPLEMENTAL DATA

Supplemental Fig. S1: https://doi.org/10.6084/m9.figshare.15826077; Supplemental Fig. S2: https://doi.org/10.6084/m9.figshare.15830391; see Supplemental Fig. S3: https://doi.org/10.6084/m9.figshare.15830526; Supplemental Fig. S4: https://doi.org/10.6084/m9.figshare.15830532; Supplemental Fig. S5: https://doi.org/10.6084/m9.figshare.15830538; Supplemental Fig. S6: https://doi.org/10.6084/m9.figshare.16617658.

ACKNOWLEDGMENTS

The authors thank the members of the Ling laboratory for providing helpful feedback and comments on this work.

GRANTS

This work was funded by the National Institutes of Health (NIH) Grant EY028163 to S. Ling and involved the use of instrumentation funded by the National Science Foundation (NSF) Major Research Instrumentation Grant 1625552.

DISCLOSURES

No conflicts of interest, financial or otherwise, are declared by the authors.

AUTHOR CONTRIBUTIONS

M.K., I.M.B., and S.L. conceived and designed research; M.K. and I.M.B. performed experiments; M.K. and I.M.B. analyzed data; M.K., I.M.B. and S.L. interpreted results of experiments; M.K. prepared figures; M.K. drafted manuscript; M.K., I.M.B., and S.L. edited and revised manuscript; M.K., I.M.B., and S.L. approved final version of manuscript.

ENDNOTE

At the request of the authors, readers are herein alerted to the fact that additional materials related to this manuscript may be found at https://osf.io/bcyp5/. These materials are not a part of this manuscript and have not undergone peer review by the American Physiological Society (APS). APS and the journal editors take no responsibility for these materials, for the website address, or for any links to or from it.

REFERENCES

1. **Carandini M**, **Heeger DJ.** Normalization as a canonical neural computation. *Nat Rev Neurosci* 13: 51–62, 2011 [Erratum in *Nat Rev Neurosci* 14: 152, 2013]. doi:10.1038/nrn3136.
2. **Coen-Cagli R**, **Kohn A**, **Schwartz O.** Flexible gating of contextual influences in natural vision. *Nat Neurosci* 18: 1648–1655, 2015. doi:10.1038/nn.4128.
3. **Schwartz O**, **Simoncelli EP.** Natural signal statistics and sensory gain control. *Nat Neurosci* 4: 819–825, 2001. doi:10.1038/90526.
4. **Simoncelli EP**, **Olshausen BA.** Natural image statistics and neural representation. *Annu Rev Neurosci* 24: 1193–1216, 2001. doi:10.1146/annurev.neuro.24.1.1193.
5. **Carandini M**, **Heeger DJ**, **Movshon JA.** Linearity and normalization in simple cells of the macaque primary visual cortex. *J Neurosci* 17: 8621–8644, 1997. doi:10.1523/JNEUROSCI.17-21-08621.1997.
6. **Cavanaugh JR**, **Bair W**, **Movshon JA.** Nature and interaction of signals from the receptive field center and surround in macaque V1 neurons. *J Neurophysiol* 88: 2530–2546, 2002. doi:10.1152/jn.00692.2001.
7. **Flevaris AV**, **Murray SO.** Attention determines contextual enhancement versus suppression in human primary visual cortex. *J Neurosci* 35: 12273–12280, 2015. doi:10.1523/JNEUROSCI.1409-15.2015.
8. **Heeger DJ.** Normalization of cell responses in cat striate cortex. *Vis Neurosci* 9: 181–197, 1992. doi:10.1017/S0952523800009640.
9. **Ni AM**, **Ray S**, **Maunsell JHR.** Tuned normalization explains the size of attention modulations. *Neuron* 73: 803–813, 2012. doi:10.1016/j.neuron.2012.01.006.
10. **Self MW**, **Lorteije JAM**, **Vangeneugden J**, **van Beest EH**, **Grigore ME**, **Levelt CN**, **Heimel JA**, **Roelfsema PR.** Orientation-tuned surround suppression in mouse visual cortex. *J Neurosci* 34: 9290–9304, 2014. doi:10.1523/JNEUROSCI.5051-13.2014.
11. **Shushruth S**, **Nurminen L**, **Bijanzadeh M**, **Ichida JM**, **Vanni S**, **Angelucci A.** Different orientation tuning of near- and far-surround suppression in macaque primary visual cortex mirrors their tuning in human perception. *J Neurosci* 33: 106–119, 2013. doi:10.1523/JNEUROSCI.2518-12.2013.
12. **Tsai JJ**, **Wade AR**, **Norcia AM.** Dynamics of normalization underlying masking in human visual cortex. *J Neurosci* 32: 2783–2789, 2012. doi:10.1523/JNEUROSCI.4485-11.2012.
13. **Xing J**, **Heeger DJ.** Center-surround interactions in foveal and peripheral vision. *Vision Res* 40: 3065–3072, 2000. doi:10.1016/S0042-6989(00)00152-8.
14. **Rabinowitz NC**, **Willmore BDB**, **Schnupp JWH**, **King AJ.** Contrast gain control in auditory cortex. *Neuron* 70: 1178–1191, 2011. doi:10.1016/j.neuron.2011.04.030.
15. **Louie K**, **Grattan LE**, **Glimcher PW.** Reward value-based gain control: divisive normalization in parietal cortex. *J Neurosci* 31: 10627–10639, 2011. doi:10.1523/JNEUROSCI.1237-11.2011.
16. **Bloem IM**, **Ling S.** Normalization governs attentional modulation within human visual cortex. *Nat Commun* 10: 5660, 2019. doi:10.1038/s41467-019-13597-1.
17. **Petrov Y**, **Carandini M**, **McKee S.** Two distinct mechanisms of suppression in human vision. *J Neurosci* 25: 8704–8707, 2005. doi:10.1523/JNEUROSCI.2871-05.2005.
18. **Trott AR**, **Born RT.** Input-gain control produces feature-specific surround suppression. *J Neurosci* 35: 4973–4982, 2015. doi:10.1523/JNEUROSCI.4000-14.2015.
19. **Bloem IM**, **Watanabe YL**, **Kibbe MM**, **Ling S.** Visual memories bypass normalization. *Psychol Sci* 29: 845–856, 2018. doi:10.1177/0956797617747091.
20. **Schallmo M-P**, **Murray SO.** Identifying separate components of surround suppression. *J Vis* 16: 2, 2016. doi:10.1167/16.1.2.
21. **Angelucci A**, **Bijanzadeh M**, **Nurminen L**, **Federer F**, **Merlin S**, **Bressloff PC.** Circuits and mechanisms for surround modulation in visual cortex. *Annu Rev Neurosci* 40: 425–451, 2017. doi:10.1146/annurev-neuro-072116-031418.
22. **Coen-Cagli R**, **Dayan P**, **Schwartz O.** Cortical surround interactions and perceptual salience via natural scene statistics. *PLoS Comput Biol* 8: e1002405, 2012. doi:10.1371/journal.pcbi.1002405.
23. **Geisler WS**, **Perry JS**, **Super BJ**, **Gallogly DP.** Edge co-occurrence in natural images predicts contour grouping performance. *Vision Res* 41: 711–724, 2001. doi:10.1016/S0042-6989(00)00277-7.

24. **Webb BS**, **Dhruv NT**, **Solomon S**, **Tailby C**, **Lennie P.** Early and late mechanisms of surround suppression in striate cortex of macaque. *J Neurosci* 25: 11666–11675, 2005. doi:10.1523/JNEUROSCI.3414-05.2005.
25. **Ling S**, **Pratte MS**, **Tong F.** Attention alters orientation processing in the human lateral geniculate nucleus. *Nat Neurosci* 18: 496–498, 2015. doi:10.1038/nn.3967.
26. **Poltoratski S**, **Ling S**, **McCormack D**, **Tong F.** Characterizing the effects of feature salience and top-down attention in the early visual system. *J Neurophysiol* 118: 564–573, 2017. doi:10.1152/jn.00924.2016.
27. **McDonald JS**, **Seymour KJ**, **Schira MM**, **Spehar B**, **Clifford CWG.** Orientation-specific contextual modulation of the fMRI BOLD response to luminance and chromatic gratings in human visual cortex. *Vision Res* 49: 1397–1405, 2009. doi:10.1016/j.visres.2008.12.014.
28. **Chen C-C.** Partitioning two components of BOLD activation suppression in flanker effects. *Front Neurosci* 8: 149, 2014. doi:10.3389/fnins.2014.00149.
29. **Pihlaja M**, **Henriksson L**, **James AC**, **Vanni S.** Quantitative multifocal fMRI shows active suppression in human V1. *Hum Brain Mapp* 29: 1001–1014, 2008. doi:10.1002/hbm.20442.
30. **Joo SJ**, **Boynton GM**, **Murray SO.** Long-range, pattern-dependent contextual effects in early human visual cortex. *Curr Biol* 22: 781–786, 2012. doi:10.1016/j.cub.2012.02.067.
31. **Williams AL**, **Singh KD**, **Smith AT.** Surround modulation measured with functional MRI in the human visual cortex. *J Neurophysiol* 89: 525–533, 2003. doi:10.1152/jn.00048.2002.
32. **Sigman M**, **Cecchi GA**, **Gilbert CD**, **Magnasco MO.** On a common circle: natural scenes and Gestalt rules. *Proc Natl Acad Sci USA* 98: 1935–1940, 2001. doi:10.1073/pnas.031571498.
33. **Vinje WE**, **Gallant JL.** Sparse coding and decorrelation in primary visual cortex during natural vision. *Science* 287: 1273–1276, 2000. doi:10.1126/science.287.5456.1273.
34. **Moeller S**, **Yacoub E**, **Olman CA**, **Auerbach E**, **Strupp J**, **Harel N**, **Uğurbil K.** Multiband multislice GE-EPI at 7 tesla, with 16-fold acceleration using partial parallel imaging with application to high spatial and temporal whole-brain fMRI. *Magn Reson Med* 63: 1144–1153, 2010. doi:10.1002/mrm.22361.
35. **Xu J**, **Moeller S**, **Auerbach EJ**, **Strupp J**, **Smith SM**, **Feinberg DA**, **Yacoub E**, **Uğurbil K.** Evaluation of slice accelerations using multiband echo planar imaging at 3T. *Neuroimage* 83: 991–1001, 2013. doi:10.1016/j.neuroimage.2013.07.055.
36. **Kriegeskorte N**, **Mur M**, **Ruff DA**, **Kiani R**, **Bodurka J**, **Esteky H**, **Tanaka K**, **Bandettini PA.** Matching categorical object representations in inferior temporal cortex of man and monkey. *Neuron* 60: 1126–1141, 2008. doi:10.1016/j.neuron.2008.10.043.
37. **Kay KN**, **Winawer J**, **Mezer A**, **Wandell BA.** Compressive spatial summation in human visual cortex. *J Neurophysiol* 110: 481–494, 2013. doi:10.1152/jn.00105.2013.
38. **Benson NC**, **Jamison KW**, **Arcaro MJ**, **Vu AT**, **Glasser MF**, **Coalson TS**, **Van Essen DC**, **Yacoub E**, **Ugurbil K**, **Winawer J**, **Kay K.** The Human Connectome Project 7 Tesla retinotopy dataset: description and population receptive field analysis. *J Vis* 18: 23, 2018. doi:10.1167/18.13.23.
39. **Andersson JLR**, **Skare S**, **Ashburner J.** How to correct susceptibility distortions in spin-echo echo-planar images: application to diffusion tensor imaging. *Neuroimage* 20: 870–888, 2003. doi:10.1016/S1053-8119(03)00336-7.
40. **Smith SM**, **Jenkinson M**, **Woolrich MW**, **Beckmann CF**, **Behrens TEJ**, **Johansen-Berg H**, **Bannister PR**, **De Luca M**, **Drobnjak I**, **Flitney DE**, **Niazy RK**, **Saunders J**, **Vickers J**, **Zhang Y**, **De Stefano N**, **Brady JM**, **Matthews PM.** Advances in functional and structural MR image analysis and implementation as FSL. *Neuroimage* 23 *Suppl 1*: S208–S219, 2004. doi:10.1016/j.neuroimage.2004.07.051.
41. **Greve DN**, **Fischl B.** Accurate and robust brain image alignment using boundary-based registration. *NeuroImage* 48: 63–72, 2009. doi:10.1016/j.neuroimage.2009.06.060.
42. **Fischl B.** FreeSurfer. *NeuroImage* 62: 774–781, 2012. doi:10.1016/j.neuroimage.2012.01.021.
43. **Reuter M**, **Rosas HD**, **Fischl B.** Highly accurate inverse consistent registration: a robust approach. *Neuroimage* 53: 1181–1196, 2010. doi:10.1016/j.neuroimage.2010.07.020.
44. **Carrasco M**, **Talgar CP**, **Cameron EL.** Characterizing visual performance fields: effects of transient covert attention, spatial frequency, eccentricity, task and set size. *Spat Vis* 15: 61–75, 2001. doi:10.1163/15685680152692015.
45. **Himmelberg MM**, **Winawer J**, **Carrasco M.** Stimulus-dependent contrast sensitivity asymmetries around the visual field. *J Vis* 20: 18, 2020. doi:10.1167/jov.20.9.18.
46. **Kupers ER**, **Carrasco M**, **Winawer J.** Modeling visual performance differences 'around' the visual field: a computational observer approach. *PLoS Comput Biol* 15: e1007063, 2019. doi:10.1371/journal.pcbi.1007063.
47. **Cannon MW**, **Fullenkamp SC.** Spatial interactions in apparent contrast: inhibitory effects among grating patterns of different spatial frequencies, spatial positions and orientations. *Vision Res* 31: 1985–1998, 1991. doi:10.1016/0042-6989(91)90193-9.
48. **Phillips DJ**, **McDougall TJ**, **Dickinson JE**, **Badcock DR.** Motion direction tuning in centre-surround suppression of contrast. *Vision Res* 179: 85–93, 2021. doi:10.1016/j.visres.2020.11.001.
49. **Zenger-Landolt B**, **Heeger DJ.** Response suppression in V1 agrees with psychophysics of surround masking. *J Neurosci* 23: 6884–6893, 2003. doi:10.1523/JNEUROSCI.23-17-06884.2003.
50. **Kastner S**, **De Weerd P**, **Desimone R**, **Ungerleider LG.** Mechanisms of directed attention in the human extrastriate cortex as revealed by functional MRI. *Science* 282: 108–111, 1998. doi:10.1126/science.282.5386.108.
51. **Tootell RBH**, **Hadjikhani NK**, **Vanduffel W**, **Liu AK**, **Mendola JD**, **Sereno MI**, **Dale AM.** Functional analysis of primary visual cortex (V1) in humans. *Proc Natl Acad Sci USA* 95: 811–817, 1998. doi:10.1073/pnas.95.3.811.
52. **Ling S**, **Blake R.** Suppression during binocular rivalry broadens orientation tuning. *Psychol Sci* 20: 1348–1355, 2009. doi:10.1111/j.1467-9280.2009.02446.x.
53. **Maloney RT**, **Clifford CWG.** Orientation anisotropies in human primary visual cortex depend on contrast. *Neuroimage* 119: 129–145, 2015. doi:10.1016/j.neuroimage.2015.06.034.
54. **Bell J**, **Badcock DR.** Luminance and contrast cues are integrated in global shape detection with contours. *Vision Res* 48: 2336–2344, 2008. doi:10.1016/j.visres.2008.07.015.